ACS Catalysis

Research Article

pubs.acs.org/acscatalysis

Insight into the Enhanced Selectivity of Phosphate-Modified Annealed Nanodiamond for Oxidative Dehydrogenation Reactions

Xiaoyan Sun,[†] Yuxiao Ding,[†] Bingsen Zhang,[†] Rui Huang,[†] De Chen,[‡] and Dang Sheng Su*,[†]

[†]Shenyang National Laboratory for Materials Science, Institute of Metal Research, Chinese Academy of Sciences, Shenyang 110016, People's Republic of China

[‡]Department of Chemical Engineering, Norwegian University of Science and Technology, Trondheim 7491, Norway

Supporting Information

ABSTRACT: Due to a lack of fundamental understanding of the surface properties of nanocarbons, tuning their surface active sites for higher selectivity of oxidative dehydrogenation reactions has always been a great challenge for carbon catalysis. In this contribution, annealed nanodiamond was controllably grafted by phosphate, which was demonstrated to be an efficient way to adjust the nanodiamond surface and significantly improve the propene selectivity in the oxidative dehydrogenation reaction. We conducted an in-depth study to explore the role of phosphate modification in the reaction in terms of the interactions between phosphate and carbon surface, the evolution and preferential location of phosphorus species, the promotion mechanism, and the impact on the reaction pathway. The results revealed that phosphate preferentially reacts with the phenol groups initially present on the nanodiamond surface, and then it selectively blocks the defect sites that lead to COx formation with an increased propene selectivity. During this process, the catalyst active sites (ketonic carbonyl groups) were not affected. Such effects originated from the formation of covalent C−O−P bonds on the carbon surface, which was estimated as 15 wt % loading.

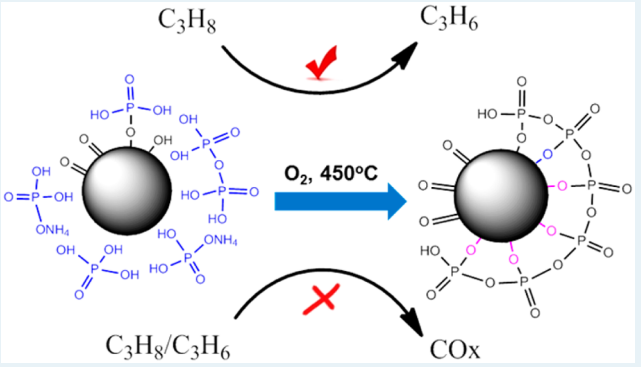

KEYWORDS: *nanodiamond, phosphate, high selectivity, oxidative dehydrogenation, mechanism*

INTRODUCTION

With the increasing development of metal-free carbon-based catalysis in recent years,[1] detonation nanodiamond (ND) as a new sp^3-hybridized carbon material has found applications in catalysis not only as a support[2] but also as an effective catalyst.[3] ND nanoparticles are composed of a crystalline diamond core with a curved graphene-like surface, and the structural defects on the surface are saturated by a large number of oxygen groups.[4] A distinct feature of NDs among the graphitic nanocarbons is that they possess more dangling bonds and higher surface energy due to the high ratio of surface atoms, thus endowing them with superior surface reactivity.[5] It has been reported that, in the direct dehydrogenation (DH) of ethylbenzene, ND showed comparable catalytic performance at a temperature lower than that for the conventional metal-based catalysts.[6]

For the industrially relevant oxidative dehydrogenation reaction (ODH), nanocarbons are regarded as promising alternative metal-free catalysts owing to their unique controllability of physical and chemical properties.[7,8] It is found that carbon nanofibers (CNFs),[9] carbon nanotubes (CNTs),[10] graphene,[11] and nanodiamond[12] can all catalyze ODH reactions without heavy carbon deposition or coke formation. The ketonic carbonyl groups on the carbon surface have been identified as the active sites for alkene production.[13,14] However, under oxidative reaction conditions, the inevitable presence of acidic oxygen species could ultimately lead to the deep oxidation of both the alkanes and alkenes by attack of the carbon chain through these oxygen species, thus significantly reducing the product selectivity.[15] Therefore, regulating the surface chemical properties of nanocarbon catalysts, especially the nature of oxygen functional groups and defective sites, plays a crucial role for improving the selectivity of the oxidative dehydrogenation reaction. Incorporation and modification of heteroatoms, such as nitrogen, boron, sulfur, and/or phosphorus, into carbon materials have been proven to be an effective method for tailoring the electronic structure and surface properties of carbon materials.[16] As for the ODH reaction, the positive impacts on boosting selectivity by phosphorus have been described on CNTs and CNFs in the ODH of ethane, propane, and *n*-butane.[7,17−19] Kinetic studies demonstrated that phosphorus can increase the selectivity by suppressing the combustion rate, rather than enhancing the formation rate of alkenes. However, no direct evidence was

Received: September 19, 2014
Revised: March 5, 2015
Published: March 9, 2015

DOI: 10.1021/acscatal.5b00042
ACS Catal. 2015, 5, 2436−2444

given in previous studies about the chemical nature of phosphorus and the exact promotion mechanism for the selectivity. The exploration of these issues is crucial for understanding the role of heteroatoms in the complex surface reactions, which could provide principles for rational design of catalysts to achieve higher selectivity. Herein, a series of phosphate-modified annealed nanodiamonds were prepared and thoroughly probed as catalysts for ODH of propane. In the ODH reaction, we focused on revealing the most important mechanistic aspects of the phosphate-interfered ODH process, including the nature of promotion effects by phosphate, the evolution of phosphorus species, and the interaction between phosphate and the carbon surface.

RESULTS AND DISCUSSION

Structure and Surface Chemistry of Phosphate-Modified Annealed Nanodiamond. It was reported that the fresh ND surface covered by an unstable disordered carbon layer tended to transform into onionlike carbon under oxidative reaction conditions.[12] Herein, ND was annealed at 1000 °C (referred to as AND) as the initial sample for phosphate modification, the surface of which has been formed as one or two curved graphitic layers (see Figure 1a). The obtained

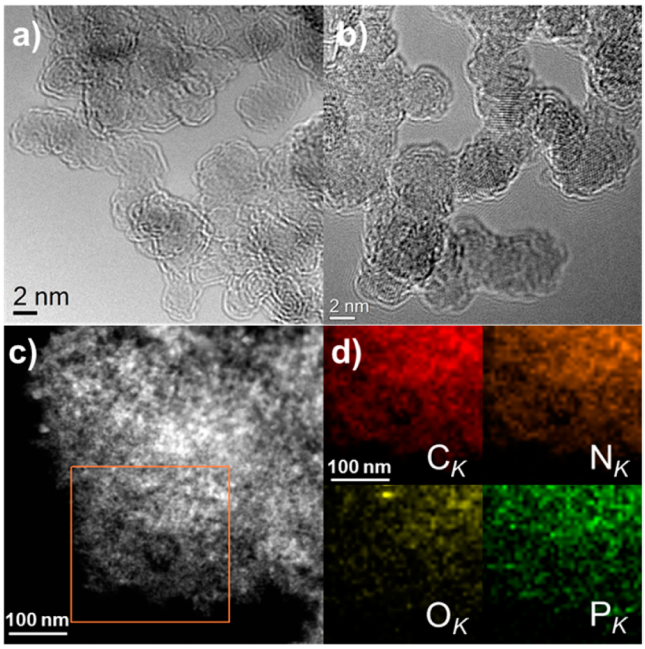

Figure 1. TEM images of (a) initial AND and (b) 12P-AND and (c) STEM image and (d) EDX elemental mapping of 12P-AND. The mapping was obtained in the boxed area in (c).

conjugated graphitic structure can also favor the covalent surface functionalization.[20] Phosphate-modified samples were synthesized by the incipient-wetness impregnation method using diammonium phosphate as precursor. The loading amount ranged from 1 to 20 wt %, which is calculated as the weight of P_2O_5 (denoted as xP-AND, with x = 1−20). The subsequent drying at 120 °C did not involve any loss of phosphate content. High-resolution transmission electron microscopy (HRTEM) image (Figure 1b) shows that phosphate treatment did not affect the AND morphology. Energy-dispersive X-ray spectroscopy (EDX) elemental maps (Figures 1c,d) show P, N, and O uniformly dispersed on the AND surface, in which N resulted from the impregnation precursor. Even for a relatively high loading, such as 20 wt % (Figure S1 in the Supporting Information), no phosphate clusters or agglomerations were observed.

Thermogravimetric analysis (TGA) is given in Figure 2a. The initial AND shows 6% weight loss, which is attributed to the desorption of surface oxygen groups. The weight loss of phosphate-modified samples correspondingly increases with increasing impregnation ratio. Meanwhile, the amounts of water and ammonia desorbed below 500 °C are consistent with the calculated weight percentages in the precursor of diammonium phosphate, confirming no phosphate loss during the preparation. Temperature-programmed oxidation (TPO) profiles (Figure 2b) reveal an increasing resistance to oxidation with higher phosphate content, and the residuals may result from the incombustible impurities of AND and the precursor salt. The oxidation temperature can be improved by 70−170 °C ($T_{50\%}$) in comparison to the temperature needed for the unmodified sample. This provides the possibility of performing the ODH reaction at relatively higher temperatures without carbon combustion.

The chemical state of phosphorus species was characterized by diffuse-reflectance infrared Fourier transform (DRIFT) spectroscopy (Figure 2c). With increasing phosphate loading, the broad bands in the region 800−1300 cm^{-1} become more predominant and slightly shift to higher wavenumbers in comparison to those of diammonium phosphate. The reason could be the contribution of the stretching vibration of phosphate-containing groups, including C−O−P (1250 cm^{-1}), P═O (1090 cm^{-1}), and P−O−P (975 cm^{-1}).[21] This indicates that a chemical bond was formed between phosphate and the carbon surface during the preparation process. Accordingly, the vibration modes of N−H groups (1400−1500 cm^{-1}) can be attributed to the undecomposed precursor adsorbed on the AND surface. Raman spectra (Figure S2 in the Supporting Information) show negligible changes in the peak position and intensity of the sp^3-diamond band at 1320 cm^{-1} and G band centered at 1580 cm^{-1}, indicating no structural impact by the modification process. The solid-state ^{31}P magic-angle spinning (MAS) NMR spectra of phosphate-modified samples show broad peaks at around 1 ppm similar to those for the precursor salt (Figure 2d), which are attributable to the orthophosphate sites $P(O)(OH)_3$ derived from diammonium phosphate. A new resonance signal centered at −11 ppm for phosphate-modified ANDs suggests the presence of surface polyphosphate units linked together by a P−O−P bond.[21] The ratio of the −11 and 1 ppm peaks is constant when the loading amount of phosphate was less than 15 wt % but decreased for 20P-AND. It seems that, when a certain value is exceeded, the excess phosphorus could not form relatively more polyphosphate structures that are covalently linked by P−O−P.

Catalytic Properties and the Role of Phosphate. Propane ODH was performed to investigate the modification effect on the catalytic activity of ANDs. By impregnation of an identical phosphorus precursor on SBA-15, no catalytic activity of phosphorus for the ODH reaction was demonstrated under the given conditions. In order to directly compare the catalytic activity derived from nanodiamonds, the catalyst weight used in the reaction was normalized to the same mass of AND. With an increase in phosphate loading, the selectivity to propene significantly improved from 45% to 70%; concomitantly, the formation of carbon oxides (COx) remarkably decreased (Figure 3a). This demonstrates that phosphate modification

DOI: 10.1021/acscatal.5b00042
ACS Catal. 2015, 5, 2436−2444

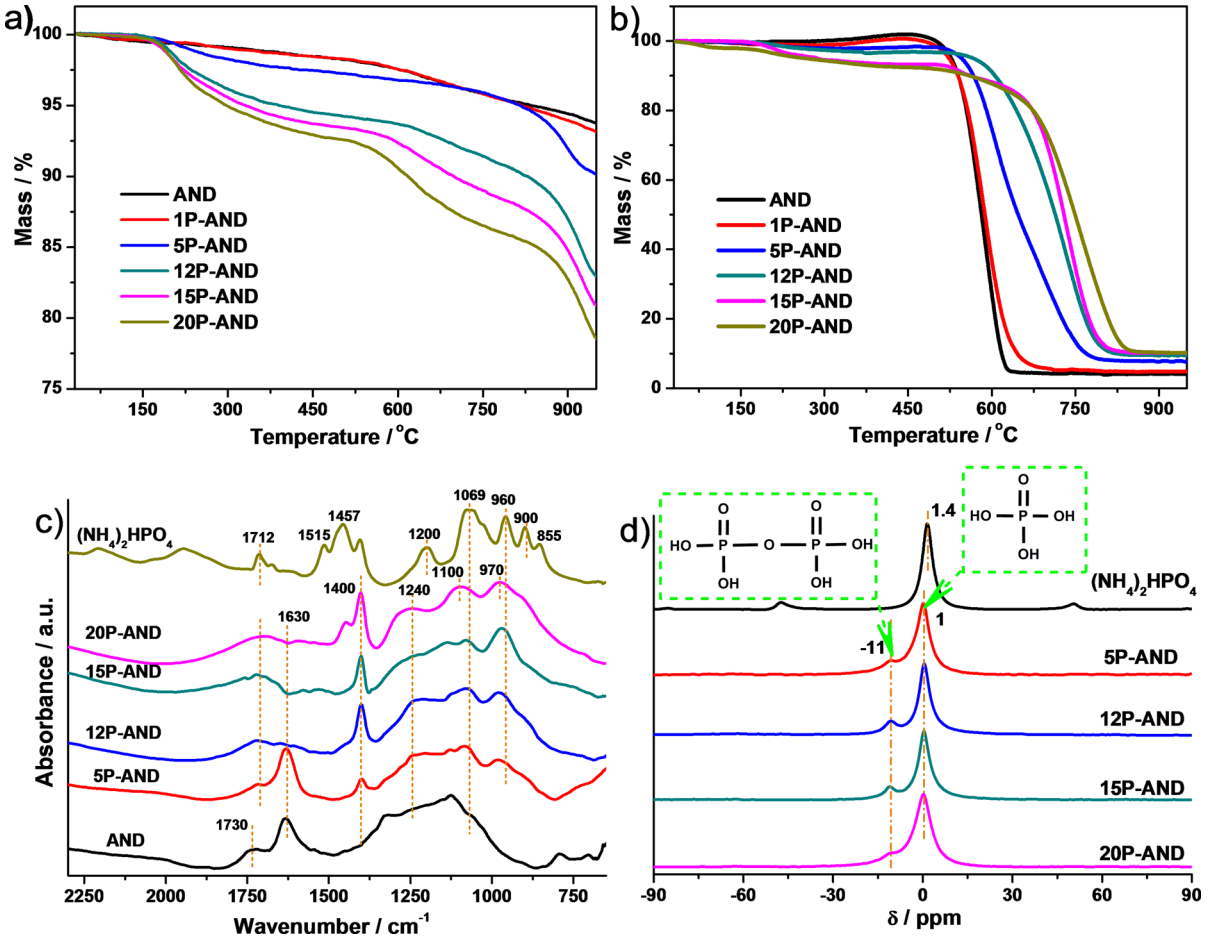

Figure 2. (a) TGA and (b) dynamic TPO curves of unmodified and phosphate-modified ANDs. Treatment conditions: from room temperature to 950 °C under argon and air flow, respectively, heating rate 10 °C min^{-1}. (c) DRIFT and (d) ^{31}P NMR spectra of unmodified and phosphate-modified ANDs, in which the spectrum of diammonium phosphate is shown as reference.

is an efficient method to adjust the AND surface for higher selectivity. Figure 3b shows the isothermal TPO curves recorded at 500 °C. Initial AND was found to be completely burned under the oxidizing atmosphere, thus severely limiting its application to high-temperature reactions. However, after phosphate modification, the sample shows a high oxidative stability at 500 °C. Therefore, in a long-term ODH reaction performed at 500 °C (Figure 3c), the phosphate-modified catalyst can provide a stable catalytic performance for a time on stream of 20 h with a conversion higher than 20%, the selectivity remaining above 45%. It should be mentioned that this selectivity shows a significant decrease in comparison to that of the reaction performed at relatively low temperature (450 °C, Figure 3a), although the carbon mass balance was still within 100 ± 0.5%. To check the structural integrity of the catalysts after the reaction, two samples reacted at 450 and 500 °C were characterized by temperature-programmed desorption (TPD) and NMR (Figure S3 in the Supporting Information). There are only small changes in the surface properties between the two catalysts, regardless of a slight decrease in the CO_2 desorption after the reaction at 500 °C (the attribution of each peak in the TPD and NMR will be discussed in detail below). Therefore, the possible reason for the decrease in selectivity at a higher temperature could be the parallel and consecutive reaction pathway of ODH, which has been reported for both carbon catalysts and metal oxide catalysts.[22,23] That is, due to the higher activation energy for COx formation from alkenes, in comparison to that of alkene formation from reactant alkanes, raising the reaction temperature would be more sensitive for the pathway with higher activation energy. This results in a significant increase in the oxidation reaction rate with a decreased selectivity. However, in comparison to the metal oxide catalysts, which need to be used at elevated temperatures,[24] the performance of phosphate-modified AND catalyst was rather moderate and stable with the advantage of no carbon deposition or catalyst deactivation during reaction.

Since phosphate modification can efficiently adjust the AND surface to significantly improve propene selectivity, the important question to be asked is as follows: what form of interactions take place between AND and phosphate? From the TGA analysis (Figure 2a), it can be determined that the precursor phosphate salt was completely decomposed by releasing water and ammonia below the reaction temperature (450 °C), resulting in mainly phosphorus oxide adsorbed on the carbon surface. TGA profiles in Figure 3d show almost no weight change during the isothermal stage of 450 °C in air until phosphate loading was up to 15 wt %, suggesting a highly stable interaction between phosphate and the AND surface. In contrast, in the case of 20P-AND, an obvious weight loss during the isothermal stage can be observed. This suggests that 15 wt % phosphate may be exactly sufficient to occupy all of the available combustion sites on the AND surface. For 20P-AND, due to the limited accessible attachment sites, the excess phosphorus is unstable and could desorb or decompose during

DOI: 10.1021/acscatal.5b00042
ACS Catal. 2015, 5, 2436−2444

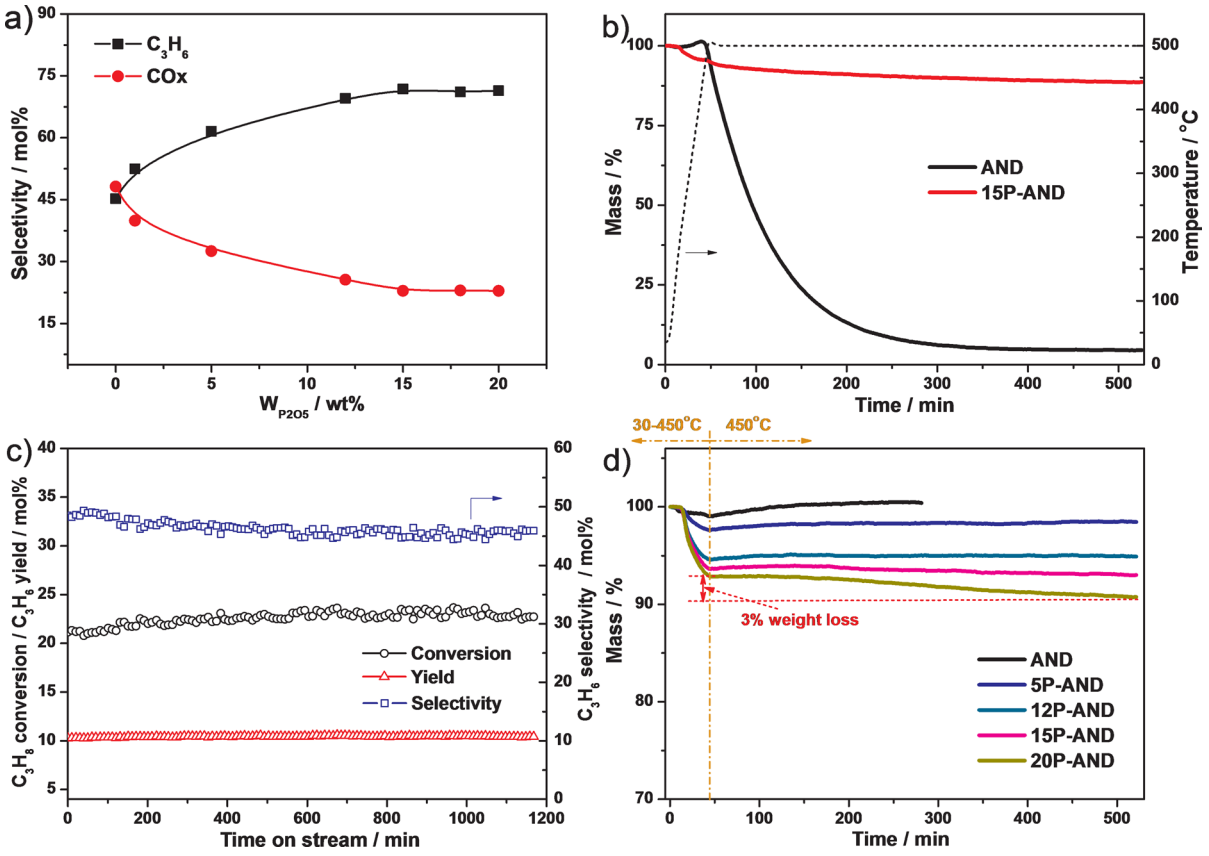

Figure 3. (a) Propene and COx selectivity as a function of P_2O_5 loading ($W_{P_2O_5}$). Reaction conditions: 450 °C, catalyst weight 150−180 mg, C_3H_8/O_2/He = 1/1/31.3. (b) Isothermal TPO curves recorded at 500 °C. (c) Long-term catalytic activity of 15P-AND conducted at 500 °C. Reaction conditions: catalyst weight 250 mg, C_3H_8/O_2/He = 1/1/31.3. (d) TGA profiles from room temperature to 450 °C (under argon flow) and at 450 °C for 8 h (the flowing gas was switched from argon to air).

the reaction. This also explains why 20P-AND showed catalytic activity similar to that of 15P-AND (Figure 3a).

It should be that the low sublimation temperature of phosphorus oxide makes it unlikely that it would exist as a separate phase under the reaction conditions. Therefore, the stable interaction, up to 15 wt % of phosphorus oxide, may come from the formation of chemical bonds with the carbon surface, resulting from C−O−P or C−P−O bonding,[25,26] which can evolve at the heating stage to 450 °C or during the reaction. Characterization of the catalysts after the reaction can reveal the chemical nature and evolution of phosphorus-containing groups. Figure 4a displays similar TGA thermograms for all used phosphate-modified catalysts, indicating that the same chemical properties were formed on the AND surface during reaction. A significant weight loss between 550 and 800 °C was found in the initial AND in comparison to that of phosphate-modified samples. This is attributed to the desorption of C−O groups on the unmodified surface, while it disappears on the used phosphate-modified catalysts due to the formation of the stable C−O−P bond with the AND surface. NMR (Figure 4b) and IR (Figure 4c) spectroscopy can further confirm this chemical interaction. NMR spectra of the catalysts used display the same resonance signals at around −24 ppm, which suggests the presence of the phosphorus species featured as $P(O)(OC)(OP)_2$.[21] Correspondingly, IR spectra show the similar C−O−P vibration band at 1252 cm^{-1} and P═O band at 1097 cm^{-1}. No evidence for the formation of C−P−O species was observed after the reaction. In addition, there were negligible structural changes during the catalytic process which can be evidenced by TEM and Raman spectroscopy (Figure S4 in the Supporting Information). Phosphorus is well dispersed throughout the AND surface after the reaction, and Raman spectra show similar peak positions and intensities of sp^3 diamond band and G band in comparison to those before the reaction. Therefore, it can be concluded that forming a stable C−O−P chemical bond between the phosphate and AND may result in the selective coverage of the combustion sites, thus leading to an increased selectivity to propene.

In order to gain further insight into the role of phosphorus in the ODH reaction, the propene formation rates for different phosphate loadings are given in Figure 4d. Interestingly, it can be found that the formation rate of propene slightly decreased to a certain extent at a low phosphate content (around 1 wt %) and stayed at the same level with increasing phosphate loading. This suggests that the phosphate should preferentially interact with a portion of ODH active sites on the AND surface under the reaction conditions, and this is followed by the blockage of the combustion sites. This interaction sequence can be further confirmed by normalizing the difference of the formation rate between propene and COx on per unit mass of phosphorus species. As shown in Figure 4d, at a low loading amount, each phosphate causes significant changes in the reaction rate due to the coverage of catalytic sites, while after these sites are occupied, the additional phosphate starts to interact with combustion sites that lead to COx formation with the same efficiency. The catalytically active sites for the ODH reaction

DOI: 10.1021/acscatal.5b00042
ACS Catal. 2015, 5, 2436−2444

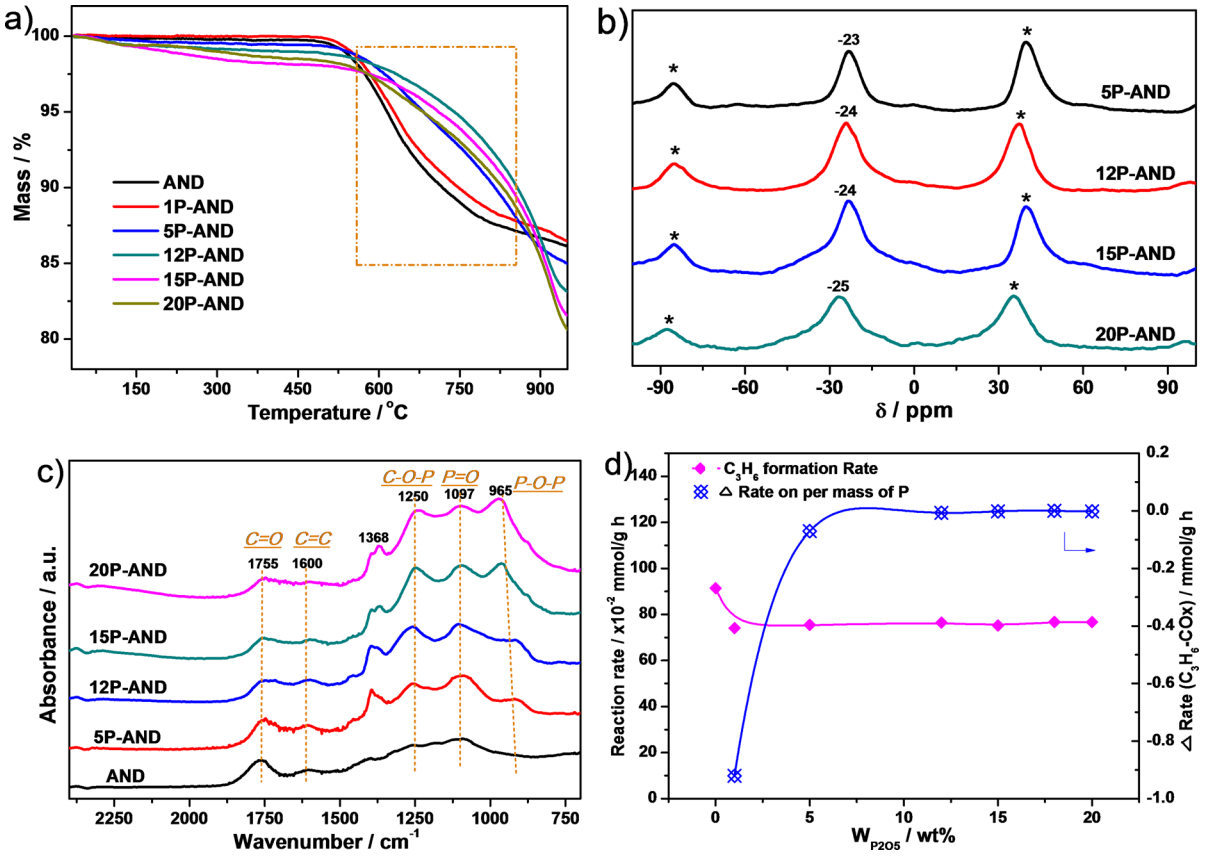

Figure 4. (a) TG curves of the catalysts used under argon flow. (b) ^{31}P NMR of phosphate-modified ANDs after the ODH reaction at 450 °C (asterisks indicate spinning side bands). (c) DRIFT spectra of ANDs after the ODH reaction at 450 °C. (d) Propene formation rate and the difference between the formation rates of propene and COx at 450 °C on per unit mass of phosphorus as a function of P_2O_5 loading ($W_{P_2O_5}$).

have been known to be the ketonic carbonyl groups, which can play the role of electron donor to activate the alkane fragment by forming phenol-like intermediates.[7] Considering the interaction between phosphate and AND, which is linked by the chemical C−O−P bond, we propose the active sites that are most likely preferentially covered by phosphate are the phenol groups, which might not be the dominating active site but could be involved in the catalytic redox process during the ODH reaction. Obviously, the phenol groups could easily form C−O−P with phosphate through the dehydration reaction (Figure S5 in the Supporting Information). In order to confirm this assumption, we quantified the amount of surface oxygen groups present on the initial AND by deconvolution of TPD spectra (Figure S5). The phenol groups can release CO upon decomposition in the temperature range 550−750 °C.[27] On this basis, the calculated amount of phenol groups is estimated to be 151 μmol/g. Assuming that one phenol group could react with one phosphate, occupying these sites would need an approximate loading of 1.1 wt % P_2O_5, which is consistent with the catalytic behavior in Figure 4d. This means that, as long as these phenol groups are covered, the reactivity could be reduced to an extent and stay at the same level with increasing phosphate content without affecting the structure of the main active sites (Figure 4d).

After some active sites were occupied, the increasing adsorption of phosphate gradually blocked certain sites for COx formation, leading to a higher selectivity toward propene (Figure 3a). The selective adsorption of phosphorus has been reported in the literature for graphite.[28] By using in situ TEM, Oh and Rodriguez found that the armchair faces of graphite were oxidized at a rate slower than that for the zigzag faces, suggesting that phosphorus species were preferentially located at armchair sites.[28] Considering the surface of annealed nanodiamond has already been formed as one or two curved graphitic layers, it is likely that the selective adsorption of phosphate observed on the AND surface follows the same rule. On the other hand, electrophilic oxygen species such as O_2^- (superoxide), and O_2^{2-} (peroxide) that are responsible for COx formation were found to favor attachment to armchair sites, for steric reasons.[29] Therefore, it is reasonable to assume that the interaction between phosphate and such sites would reduce the generation of the electrophilic oxygen groups on these defects during the reaction, leading to an increased selectivity of propene.

TPD can give quantitative evidence about the evolution of surface groups after phosphate modification and further reveal the interaction between AND and phosphate. In general, CO desorption is mainly attributed to carboxylic anhydride, phenol, and carbonyl/quinone species, whereas CO_2 desorption results from carboxylic anhydride at low temperatures and lactones at higher temperatures.[27,30−33] On this basis, CO and CO_2 desorption profiles of the catalysts used were deconvoluted to separate those distinct peaks from the decomposition of various functionalities (Figures 5a,b and Tables S1 and S2 in the Supporting Information). It is noteworthy that, after phosphate modification, the new evolution of CO_2 and CO appears in the range 800−900 °C and the desorption peaks shift to higher temperature with higher intensity with an increase in the

DOI: 10.1021/acscatal.5b00042
ACS Catal. 2015, 5, 2436−2444

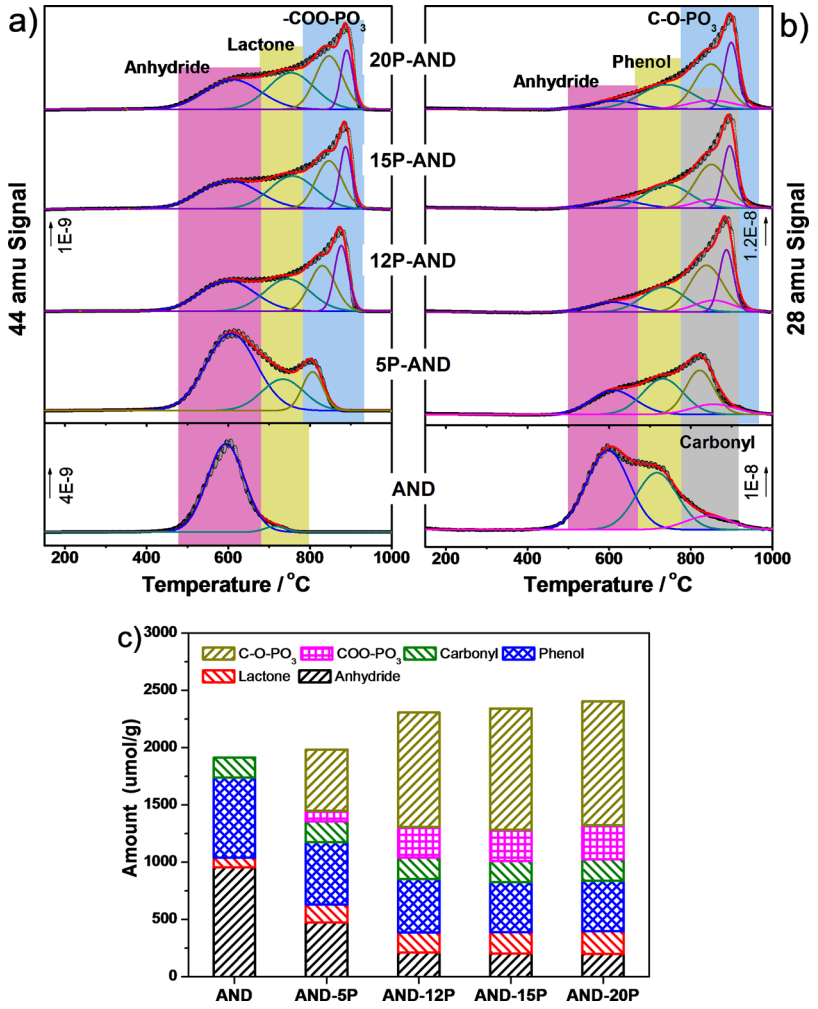

Figure 5. Deconvolution of TPD profiles of ANDs after the ODH reaction at 450 °C for (a) CO_2 desorption and (b) CO desorption. The black lines represent the original TPD curves, and the red lines represent the fitted curves. Detailed parameters for the deconvolution are given in Tables S1 and S2 in the Supporting Information. (c) Variations in the amounts of different oxygen-containing groups on the basis of the deconvoluted spectra.

phosphate loading. This phenomenon was also observed by others when using phosphoric acid to activate carbon materials.[22,34,35] Evolutions of CO_2 and CO at these high temperatures can be associated with the decomposition of the $-COO-PO_3$ and $C-O-PO_3$ groups, respectively, in which the O−P bond may be broken first at high temperature due to the relatively lower bond energy, leaving the O atom bonded to the carbon site further desorbed in the form of CO and CO_2.[34] This corroborates the formation of a C−O−P bond at the surface. The shift for those peaks is probably due to the formation of a polyphosphate structure that hinders the extraction of the phosphorus species. The amounts of different functional groups on the basis of the deconvoluted spectra are given in Figure 5c. The amounts of carbonyl groups show negligible changes, confirming that phosphate modification did not affect the active sites during the reaction. However, a decrease in the desorption of the phenol group was observed after modification due to its interaction with phosphate. More importantly, in comparison to unmodified AND, the desorption of anhydride groups was significantly reduced after modification and stayed at the same level when the loading exceeded 15 wt %. This demonstrates that phosphate mainly suppressed the formation of electrophilic oxygen species during reaction, which are responsible for COx formation. Indeed, phosphate modification generated a significant amount of groups with high thermal stability during TPD, and the cleavage of the highly stable $C-O-PO_3$ groups makes the greatest contribution. This can probably be attributed to the strong interaction of phosphate with the oxygen groups and defects on the AND surface, which can happen under the reaction conditions or could be induced by a high-temperature treatment of the TPD process. On the other hand, by comparison of the TPD spectra of phosphate-modified samples before and after the reaction (Figure S6 in the Supporting Information), the desorbed amounts of $-COO-PO_3$ and $C-O-PO_3$ groups increased after the ODH. This might be due to reactions between phosphate and electrophilic oxygen species during the ODH to form new $-COO-PO_3$ and $C-O-PO_3$ groups.[34] This can inhibit the negative effect of electrophilic oxygen species on the reaction, thus providing a higher selectivity. Meanwhile, the slightly increased desorptions of lactone and phenol groups were also observed after ODH in comparison to those before the reaction, which were formed in situ during the reaction and considered to have no contribution to the catalytic activity.

To obtain more detailed information about the reaction pathway, Figure 6a shows the linear fit of selectivity of COx and

DOI: 10.1021/acscatal.5b00042
ACS Catal. 2015, 5, 2436−2444

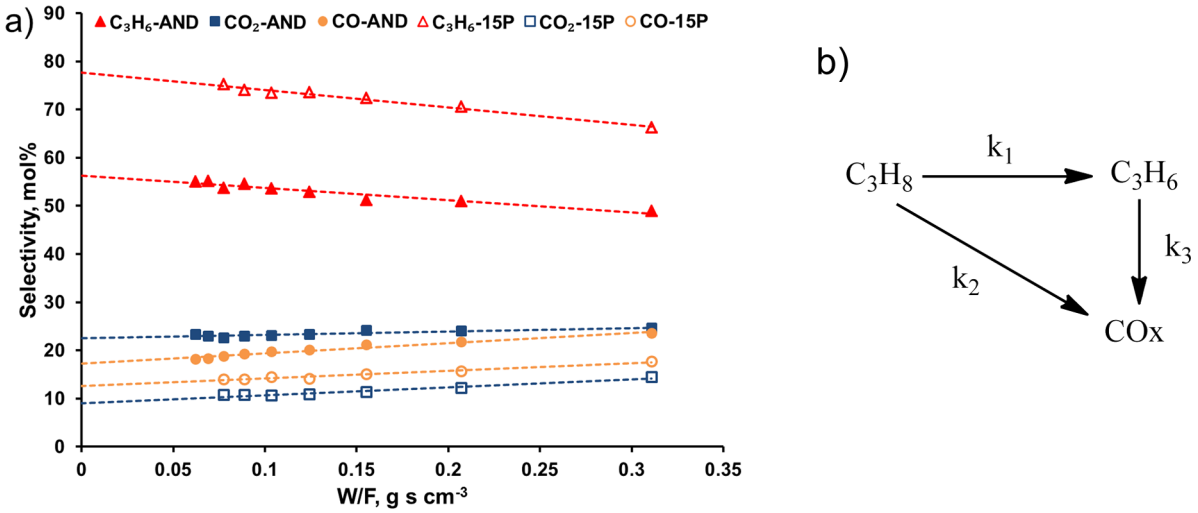

Figure 6. (a) C_3H_6 and COx selectivity at variable contact times (W/F) for AND and 15P-AND catalysts. Reaction conditions: 450 °C, catalyst weight 50 mg, 3% C_3H_8, and 3% O_2, He balance, total flow rate ranging from 10 to 50 mL/min. (b) Reaction network in the ODH of propane.

propene at variable contact times (W/F) performed on the two selected catalysts. It can be found that C_3H_6 selectivity decreases while COx selectivity increases with contact time. By examination of the zero W/F intercept of the selectivity, the primary products can be confirmed.[36] The selectivities of propene and COx at zero contact time are much larger than zero (Figure 6a), indicating that both propene and COx are primary products from propane. In addition, the selectivity of propene remarkably decreases and selectivity of COx increases almost linearly with increasing contact time. This suggests that propene is the unstable primary product and COx species are the primary and secondary stable products. On the basis of the product analysis, a reaction network of ODH is proposed as both parallel and consecutive reaction steps (Figure 6b), which is in good agreement with the previous reported network.[37] More specifically, it can be found that the selectivity of CO_2 is a weak function of contact time, indicating that CO_2 is mostly a primary product from propane. Phosphate modification of 15 wt % did not change the slope of the CO_2 selectivity curve but reduced more than 50% of the selectivity at zero contact time. This suggests that phosphate significantly suppressed CO_2 formation from the direct combustion of propane (k_2). However, CO is a primary product and a stable secondary product, since the selectivity concurrently increases with an increase in the contact time. Adding phosphate changes both the intersection and slope of the CO curve, which indicates that both k_2 and k_3 pathways for CO formation were efficiently inhibited by phosphate selective blockage.

CONCLUSION

The annealed nanodiamond was controllably modified by phosphate and used as a catalyst for the ODH reaction. The significantly enhanced oxidative stability by phosphate modification allows AND to act as an efficient metal-free catalyst for the ODH reaction at elevated temperature with a high selectivity. Furthermore, we gave a clear picture about the promotion mechanism and interaction between phosphate and AND for the first time. On the basis of combined characterizations, it is demonstrated that this promotion effect originated from the formation of a covalent C−O−P bond with the AND surface, which was highly stable during the reaction. The location of phosphate on the carbon matrix is quite selective under the reaction conditions. Phosphate preferentially interacts with the phenol groups initially present on the AND surface by dehydration. As the phosphorus content increases, it gradually occupies the defects to suppress the in situ formation of electrophilic oxygen species, thus resulting in a higher selectivity toward propene production, during which the active sites (ketonic carbonyl groups) for dehydrogenation were not affected. The reaction pathway analysis indicates that phosphate modification mainly suppresses CO_2 formation from propane and CO formation from the direct combustion and deep oxidation reaction. The results give a fundamental understanding of phosphate-modified nanocarbon for the ODH reaction. This work also provides a new direction to improve the selectivity by controllable synthesis on the termination of nanocarbon defect sites.

METHODS

Preparation of Phosphate-Modified ANDs. The ND used in this study (high-purity grade) was supplied by Beijing Grish Hitech Co. China; it was purified from the black powder produced by explosive detonation using a nitric acid/sulfuric acid/fuming sulfuric acid mixture. The diamond powder thus obtained has a light brown color with particle sizes of ca. 3−10 nm and with a phase purity of powder >98%. In order to remove the unstable disordered carbon on the surface, ND was then thermally annealed in a furnace at 1000 °C for 4 h under a helium flow (defined as AND). The modified catalysts were prepared by the incipient-wetness impregnation method. AND was soaked in a controlled amount of $(NH_4)_2HPO_4$ aqueous solution and stirred ultrasonically to a near-dryness state. The impregnated samples were then dried in air at 120 °C overnight.

Characterizations. HRTEM was performed using a FEI Cs-corrected Titan 80-300 microscope and a FEI Tecnai G2 F20 microscope. Thermogravimetric (TG) analysis was performed on a NETZSCH STA 449 F3 instrument under a flow of argon or air (50 mL min^{-1}) with a heating rate of 10 °C min^{-1}. IR studies were conducted with a Thermo Nicolet iZ10 FTIR system using a diffuse reflectance infrared Fourier transform (DRIFT) cell that has been extensively modified to allow in situ treatments up to 500 °C under flowing gases. The spectra were recorded in the 650−4000 cm^{-1} range with 128

DOI: 10.1021/acscatal.5b00042
ACS Catal. 2015, 5, 2436−2444

scans at a resolution of 4 cm^{-1}. Temperature-programmed desorption (TPD) experiments were performed under a He atmosphere. The temperature program involved heating at 10 °C/min from ambient temperature to 120 °C, at which it was kept for 40 min, and then the temperature was raised to 1000 °C at 5 °C/min. The product gases were analyzed by online MS (Pfeiffer-Balzer Omnistar); the peaks at m/z 28 and 44 were monitored for the detection of CO and CO_2 with a time resolution of 0.1 s. The integration of the peak area of evolved gases was quantified on the basis of the calibration curve built by using calcium oxalate ($CaC_2O_4 \cdot H_2O$) as a standard sample. Raman spectroscopy was performed on a LabRam HR 800 instrument using a 325 nm laser. Solid-state ^{31}P magic angle spinning (MAS) NMR characterization was performed on a Varian Infinity-plus 400 spectrometer using a 5 mm probe with a recycle delay of 5 s (ensuring a complete relaxation of all the ^{31}P signals).

Catalytic Tests. Oxidative dehydrogenation of propane (ODH) was carried out in a quartz fixed-bed reactor. Carbon catalysts were fixed between two layers of quartz wool. The gas flows were monitored by a mass controller system calibrated for each gas. The reaction temperature was set at 450 °C and controlled by a thermocouple located inside the reactor bed. The reaction products were analyzed by an Agilent 7890A gas chromatograph equipped with a flame ionization detector (FID) for hydrocarbon and a thermal conductivity detector (TCD) for inorganic components. Experiments with blanks and SBA-15 modified with phosphate showed that the reaction rates were negligible without carbon catalyst. In all tests, carbon mass balances were within 100 ± 0.5%. The reaction network analysis was performed under differential reaction conditions, and the conversion level was less than 10%, being free of heat and mass transfer limitation.

■ ASSOCIATED CONTENT

Supporting Information

The following file is available free of charge on the ACS Publications website at DOI: 10.1021/acscatal.5b00042.

EDX mapping, TEM, Raman spectra, and TPD (PDF)

■ AUTHOR INFORMATION

Corresponding Author

*D.S.S.: tel and fax, (+86)24-23971577; e-mail, dssu@imr.ac.cn.

Notes

The authors declare no competing financial interest.

■ ACKNOWLEDGMENTS

The authors sincerely acknowledge the assistances by Xiaoli Pan for TEM characterizations and Xianchun Liu from the Dalian Institute of Chemical Physics, Chinese Academy of Sciences, for NMR tests. The authors also thank Prof. Figueiredo from the University of Porto (Portugal), Dr. Rui Wang from the National Institute of Clean-and-Low-Carbon Energy, and Dr. Wei Qi and Guodong Wen for fruitful discussions. This work was supported by the Foundation from MOST (Grant Nos. 2011CBA00504), NSFC of China (Grant Nos. 21133010, 21103203, 51221264, 21261160487, 21203215), and "Strategic Priority Research Program" of the Chinese Academy of Sciences (Grant No. XDA09030103).

■ REFERENCES

(1) Su, D. S.; Perathoner, S.; Centi, G. *Chem. Rev.* **2013**, *113*, 5782−5816.
(2) Vershinin, N. N.; Efimov, O. N.; Bakaev, V. A.; Aleksenskii, A. E.; Baidakova, M. V.; Sitnikova, A. A.; Vul', A. Y. *Fullerenes, Nanotubes, Carbon Nanostruct.* **2011**, *19*, 63−68.
(3) Zhang, J.; Wang, R.; Su, D. S. *Zhongguo Kexue: Huaxue* **2012**, *42*, 406−414.
(4) Aleksenskii, A. E.; Baidakova, M. V.; Vul', A. Y.; Siklitskii, V. I. *Phys. Solid State* **1999**, *41*, 668−671.
(5) Ozawa, M.; Inaguma, M.; Takahashi, M.; Kataoka, F.; Kruger, A.; Osawa, E. *Adv. Mater.* **2007**, *19*, 1201−1206.
(6) Zhang, J.; Su, D. S.; Blume, R.; Schlogl, R.; Wang, R.; Yang, X. G.; Gajovic, A. *Angew. Chem., Int. Ed.* **2010**, *49*, 8640−8644.
(7) Zhang, J.; Liu, X.; Blume, R.; Zhang, A.; Schlogl, R.; Su, D. S. *Science* **2008**, *322*, 73−77.
(8) Su, D. S.; Zhang, J.; Frank, B.; Thomas, A.; Wang, X.; Paraknowitsch, J.; Schlogl, R. *ChemSusChem* **2010**, *3*, 169−180.
(9) Zhao, T. J.; Sun, W. Z.; Gu, X. Y.; Ronning, M.; Chen, D.; Dai, Y. C.; Yuan, W. K.; Holmen, A. *Appl. Catal., A* **2007**, *323*, 135−146.
(10) Liu, X.; Su, D. S.; Schlogl, R. *Carbon* **2008**, *46*, 547−549.
(11) Schwartz, V.; Fu, W. J.; Tsai, Y. T.; Meyer, H. M.; Rondinone, A. J.; Chen, J. H.; Wu, Z. L.; Overbury, S. H.; Liang, C. D. *ChemSusChem* **2013**, *6*, 840−846.
(12) Liu, X.; Frank, B.; Zhang, W.; Cotter, T. P.; Schlogl, R.; Su, D. S. *Angew. Chem., Int. Ed.* **2011**, *50*, 3318−3322.
(13) Pereira, M. F. R.; Orfao, J. J. M.; Figueiredo, J. L. *Appl. Catal., A* **1999**, *184*, 153−160.
(14) Macia-Agullo, J. A.; Cazorla-Amoros, D.; Linares-Solano, A.; Wild, U.; Su, D. S.; Schlogl, R. *Catal. Today* **2005**, *102*, 248−253.
(15) Pelech, I.; Soares, O. S. G. P.; Pereira, M. F. R.; Figueiredo, J. L. *Catal. Today* **2014**, DOI: 10.1016/j.cattod.2014.10.007.
(16) Serp, P.; Figueiredo, J. L. *Carbon Materials for Catalysis*; Wiley: Hoboken, NJ, 2009.
(17) Frank, B.; Zhang, J.; Blume, R.; Schlogl, R.; Su, D. S. *Angew. Chem., Int. Ed.* **2009**, *48*, 6913−6917.
(18) Frank, B.; Morassutto, M.; Schomäcker, R.; Schlögl, R.; Su, D. S. *ChemCatChem* **2010**, *2*, 644−648.
(19) Sui, Z. J.; Zhou, J. H.; Dai, Y. C.; Yuan, W. K. *Catal. Today* **2005**, *106*, 90−94.
(20) Liang, Y. J.; Meinhardt, T.; Jarre, G.; Ozawa, M.; Vrdoljak, P.; Scholl, A.; Reinert, F.; Krueger, A. *J. Colloid Interface Sci.* **2011**, *354*, 23−30.
(21) Bourbigot, S.; Lebras, M.; Delobel, R.; Breant, P.; Tremillon, J. M. *Carbon* **1995**, *33*, 283−294.
(22) Schwartz, V.; Xie, H.; Meyer, H. M.; Overbury, S. H.; Liang, C. D. *Carbon* **2011**, *49*, 659−668.
(23) Tellez, C.; Menendez, M.; Santamaria, J. *J. Catal.* **1999**, *183*, 210−221.
(24) Cavani, F.; Ballarini, N.; Cericola, A. *Catal. Today* **2007**, *127*, 113−131.
(25) Mckee, D. W. *Carbon* **1972**, *10*, 491−492.
(26) Imamura, R.; Matsui, K.; Takeda, S.; Ozaki, J.; Oya, A. *Carbon* **1999**, *37*, 261−267.
(27) Figueiredo, J. L.; Pereira, M. F. R.; Freitas, M. M. A.; Orfao, J. J. M. *Carbon* **1999**, *37*, 1379−1389.
(28) Oh, S. G.; Rodriguez, N. M. *J. Mater. Res.* **1993**, *8*, 2879−2888.
(29) Sherman, A.; Eyring, H. *J. Am. Chem. Soc.* **1932**, *54*, 2661−2675.
(30) Boehm, H. P. *Carbon* **2002**, *40*, 145−149.
(31) Zhou, J. H.; Sui, Z. J.; Zhu, J.; Li, P.; De, C.; Dai, Y. C.; Yuan, W. K. *Carbon* **2007**, *45*, 785−796.
(32) Li, N.; Ma, X. L.; Zha, Q. F.; Kim, K.; Chen, Y. S.; Song, C. S. *Carbon* **2011**, *49*, 5002−5013.
(33) Figueiredo, J. L.; Pereira, M. F. R.; Freitas, M. M. A.; Orfao, J. J. M. *Ind. Eng. Chem. Res.* **2007**, *46*, 4110−4115.
(34) Wu, X. X.; Radovic, L. R. *Carbon* **2006**, *44*, 141−151.
(35) Bedia, J.; Rosas, J. M.; Marquez, J.; Rodriguez-Mirasol, J.; Cordero, T. *Carbon* **2009**, *47*, 286−294.

DOI: 10.1021/acscatal.5b00042
ACS Catal. 2015, 5, 2436−2444

(36) Michaels, J. N.; Stern, D. L.; Grasselli, R. K. *Catal. Lett.* **1996**, *42*, 135−137.
(37) Dinse, A.; Khennache, S.; Frank, B.; Hess, C.; Herbert, R.; Wrabetz, S.; Schlogl, R.; Schomacker, R. *J. Mol. Catal. A: Chem.* **2009**, *307*, 43−50.

DOI: 10.1021/acscatal.5b00042
ACS Catal. 2015, 5, 2436−2444